J|A|C|S
ARTICLES
Published on Web 01/03/2007

Synthetic Control over Magnetic Moment and Exchange Bias in All-Oxide Materials Encapsulated within a Spherical Protein Cage

Michael T. Klem,[†,‡] Damon A. Resnick,[‡,§] Keith Gilmore,[‡,§] Mark Young,[‡,||] Yves U. Idzerda,[*,‡,§] and Trevor Douglas[*,†‡]

Contribution from the Department of Chemistry and Biochemistry, Center for Bio-Inspired Nanomaterials, Department of Physics, and Department of Plant Sciences, Montana State University, Bozeman, Montana 59717

Received September 19, 2006; E-mail: tdouglas@chemistry.montana.edu

Abstract: This work focuses on the synthetic control of magnetic properties of mixed oxide magnetic nanoparticles of the general formula $Fe_{3-x}Co_xO_4$ ($x \leq 0.33$) in the protein cage ferritin. In this biomimetic approach, variations in the chemical synthesis result in the formation of single-phase $Fe_{3-x}Co_xO_4$ alloys or intimately mixed binary phase Fe/Co oxides, modifying the chemical structure and magnetic behavior of these particles, as characterized by static and dynamic magnetization measurements and X-ray absorption spectroscopy.

Introduction

The exchange coupling between ferro/ferrimagnetic and antiferromagnetic phases in composite materials is of considerable interest for technological applications such as high-density recording and sensors.[1−5] As the nanoparticle size is decreased the magnetic anisotropy energy, responsible for holding the magnetic orientation, becomes comparable to the thermal energy. In this size regime, the thermal fluctuations induce random motion to the magnetic moment and the nanoparticles become superparamagnetic.[6] The technological drive toward miniaturization comes into direct conflict with the superparamagnetism observed in magnetic nanoparticles leading to the "superparamagnetic limit".[7,8] However, exchange coupling at the interface between ferromagnetic and antiferromagnetic materials can introduce additional magnetic anisotropy effects leading to magnetic order at higher temperatures while maintaining small particle size.

Exchange coupling was first observed in partially oxidized Co particles that were field cooled across the Néel temperature of CoO.[9] The exchange bias manifests itself in a unidirectional shifted hysteresis loop and has been used to control the magnetization in devices like magnetoresistive spin valves.[9−12] Typically, exchange bias has been studied in thin films because of the use in technological applications with examples being Fe_3O_4/CoO, Fe/FeF_2, and CoO/permalloy.[13−16] Recent work has focused on exchange bias in particulate systems, the simplest being a core material that is ferromagnetic and a shell that is antiferromagnetic.[5,14,17−19]

There is growing interest in materials chemistry in taking advantage of the physical and chemical properties of biomolecules for the development of nanoscale materials. A detailed understanding of biomineralization has generated an interest in using biomimetic approaches for the controlled synthesis of new materials.[20−23] This bioinspired approach to materials synthesis has successfully utilized well-defined protein architectures,[24−29,30a]

[†] Department of Chemistry and Biochemistry.
[‡] Center for Bio-Inspired Nanomaterials.
[§] Department of Physics.
[||] Department of Plant Sciences.

(1) Martin, J. I.; Nogues, J.; Liu, K.; Vicent, J. L.; Schuller, I. K. *J. Magn. Magn. Mater.* **2003**, *256*, 449.
(2) Sun, S. H.; Murray, C. B.; Weller, D.; Folks, L.; Moser, A. *Science* **2000**, *287*, 1989.
(3) Kodama, R. H. *J. Magn. Magn. Mater.* **1999**, *200*, 359.
(4) *Scientific and Clinnical Applications of Magnetic Materials*; Plenum: New York, 1997.
(5) Darling, S. B.; Bader, S. D. *J. Mater. Chem.* **2005**, *15*, 4189.
(6) Aharoni, A. *Introduction to the Theory of Ferromagnetism*, 2nd ed.; Oxford University Press, Inc: New York, 2000.
(7) Thompson, D. A.; Best, J. S. *IBM J. Res. Dev.* **2000**, *44*, 311.
(8) Weller, D.; Moser, A. *IEEE Trans. Magn.* **1999**, *35*, 4423.
(9) Meiklejohn, W. H.; Bean, C. P. *Phys. Rev.* **1956**, *102*, 1413.
(10) Meiklejohn, W. H.; Bean, C. P. *Phys. Rev.* **1957**, *105*, 904.
(11) Meiklejohn, W. H.; Bean, C. P. *J. Appl. Phys.* **1962**, *33*, 1328.
(12) Nogues, J.; Schuller, I. K. *J. Magn. Magn. Mater.* **1999**, *192*, 203.
(13) Cai, J. W.; Liu, K.; Chien, C. L. *Phys. Rev. B* **1999**, *60*, 72.
(14) Schuller, I. K. *MRS Bull.* **2004**, *29*, 642.
(15) Takano, K.; Kodama, R. H.; Berkowitz, A. E.; Cao, W.; Thomas, G. *Phys. Rev. Lett.* **1997**, *79*, 1130.
(16) Takano, K.; Kodama, R. H.; Berkowitz, A. E.; Cao, W.; Thomas, G. *J. Appl. Phys.* **1998**, *83*, 6888.
(17) Chakrabarti, S.; Mandal, S. K.; Chaudhuri, S. *Nanotechnology* **2005**, *16*, 506.
(18) Masala, O.; Seshadri, R. *J. Am. Chem. Soc.* **2005**, *127*, 9354.
(19) Nogues, J.; Sort, J.; Langlais, V.; Skumryev, V.; Surinach, S.; Munoz, J. S.; Baro, M. D. *Phys. Rep.-Rev. Sec. Phys. Lett.* **2005**, *422*, 65.
(20) *Biomimetic Materials Chemistry*; VCH Publishers, Inc: New York, 1996; p 383.
(21) Aizenberg, J.; Muller, D. A.; Grazul, J. L.; Hamann, D. R. *Science* **2003**, *299*, 1205.
(22) Lee, S. W.; Mao, C. B.; Flynn, C. E.; Belcher, A. M. *Science* **2002**, *296*, 892.
(23) Mann, S.; Archibald, D. D.; Didymus, J. M.; Douglas, T.; Heywood, B. R.; Meldrum, F. C.; Reeves, N. J. *Science* **1993**, *261*, 1286.
(24) Allen, M.; Willits, D.; Young, M.; Douglas, T. *Inorg. Chem.* **2003**, *42*, 6300.
(25) Douglas, T.; Dickson, D. P. E.; Betteridge, S.; Charnock, J.; Garner, C. D.; Mann, S. *Science* **1995**, *269*, 54.
(26) Douglas, T.; Strable, E.; Willits, D.; Aitouchen, A.; Libera, M.; Young, M. *Adv. Mater.* **2002**, *14*, 415.
(27) Douglas, T.; Young, M. *Nature* **1998**, *393*, 152.

macromolecular templates,[30b] and evolved molecular interactions[31] to exert synthetic control over crystal morphology, phase, and orientation. In particular, protein cage architectures having high symmetry have been shown to act as constrained reaction environments for the synthesis and encapsulation of inorganic and organic nanomaterials.[24,26−28,32]

Ferritins are ubiquitous with life and consist of 24 protein subunits that self-assemble into a cagelike architecture with an exterior diameter of 12 nm and an interior diameter of 8 nm in which a hydrated ferric oxide/phosphate is mineralized. Ferritins have evolved to sequester Fe in vivo, but the protein has been used as a template in synthetic reactions with various metal ions, which results in the formation of inorganic nanoparticles constrained exclusively within the protein cage architecture. Materials such as Fe_3O_4,[29,33−38] Co_3O_4,[24,39] Mn_3O_4,[40−42] CoPt,[43] Pd,[44] Ag,[45] CdS,[46] CdSe,[47] and ZnSe[48] have been synthesized within the ferritin cage.

In this work, synthetic control over the magnetic exchange bias behavior was exerted by using a biomimetic approach with ferritin as a size-constrained reaction vessel for the controlled synthesis of metal oxide nanoparticles containing both Fe and Co oxides. These materials exhibit significant magnetic exchange bias, and we have demonstrated that this property, as well as the magnetic moment, can be tailored by adjusting the synthesis conditions and Fe/Co ratio.

Experimental Section

Synthesis. A deaerated solution of 0.1 M NaCl (15 mL) was added to a jacketed reaction vessel under N_2 (to maintain an oxygen free environment), and 5 mg of apoferritin (Sigma) was added to the reaction vessel. The temperature was maintained at 65 °C by circulating water through the jacketed flask, and the reaction was brought to pH 8.5 using 50 mM NaOH (Brinkmann 718 AutoTitrator). A loading factor of 1000 M (M = Co or Fe) was achieved by adding deaerated solutions of iron ($(NH_4)_2Fe(SO_4)\cdot 6H_2O$ (12.5 mM)), cobalt ($Co(NO_3)_2\cdot 6H_2O$ (12.5 mM)), and H_2O_2 as an oxidant (4.17 mM) continuously and simultaneously at a constant rate (0.064 mL/min) using a syringe pump (Kd Scientific). Solutions of H_2O_2 were freshly prepared, and the concentration was determined using a permanganate titration.[49] H^+ generated during the reaction was titrated dynamically with a Brinkmann 718 automatic titrator using 50 mM NaOH. Metal ion and oxidant solutions were added over a 15 min period, at which point the reaction was considered complete.

Solutions of metal ion (Co(II)/Fe(II)) and oxidant (H_2O_2) were added via syringe pump to the apoferritin cages under an atmosphere of N_2 at pH 8.5 and elevated temperature (65 °C) over a defined time period. In the presence of apoferritin the reaction proceeded to form a homogeneous dark brown solution while control reactions performed in the absence of ferritin resulted in bulk precipitation of a dark brown solid. Dynamic light scattering of the ferritin reaction showed no apparent change in protein diameter. The lack of precipitation and the absence of any change in the exterior diameter of the protein cage suggest that the reaction occurred in a spatially selective manner within the ferritin cage. For this study, Co doping concentrations of 5%, 10%, and 33% were used in addition to single-component oxide particles of Fe_3O_4 and Co_3O_4. Metal ion addition for the 33% Co doping was performed in a slow (over 30 min) or fast (5 min) manner instead of the 15 min addition for all other samples.

Transmission Electron Microscopy (TEM). TEM data were collected on a Leo 912, with Ω filter, operating at 80 keV. Samples were concentrated using microcon ultrafilters (Microcon YM-100) with 100 kDa Mw cutoff and transferred to carbon-coated copper grids. Samples were imaged both stained with uranyl acetate and unstained. Electron diffraction data were collected on these samples, and *d*-spacing was calculated and compared to powder diffraction files for Fe_3O_4 and Co_3O_4 after calibration of the instrument with a Au standard.

Dynamic Light Scattering (DLS). Dynamic light scattering (DLS) measurements were made on a Brookhaven Instruments ZetaPals (phase analysis light scattering) particle size analyzer. DLS was measured at 90° using a 661 nm diode laser, and the correlation functions were fit using a nonnegatively constrained least-squares analysis.[50]

Magnetometry. All magnetic characterizations were performed on a Physical Properties Measurement System from Quantum Design. Static and dynamic magnetic measurements were carried out using a vibrating-sample magnetometer (VSM) and alternating current magnetic susceptibility (ACMS) options also from Quantum Design.

X-ray Absorption Spectroscopy (XAS). All XAS spectra were taken at either the MSU Nanostructured Material X-ray Characterization Facility located at beamline U4-B of the National Synchrotron Light Source or the Advanced Light Source beamline 4.0.2 at Lawrence Berkeley National Laboratory. XAS spectra of the protein cage samples presented here were taken in transmission while the spectra of the reference powder samples were taken using the electron yield technique by monitoring the sample current.

Results and Discussion

We have used the cagelike architecture of ferritin to synthesize a mixed-metal ion oxide (Co/Fe) formed under different Co:Fe ratios and synthesized under "fast" (5 min) or "slow" (30 min) conditions designed to favor either mixed ($Co_xFe_{3-x}O_4$) or segregated (Co_3O_4/Fe_3O_4) particle formation. This biomimetic synthetic approach has enabled tailoring of the exchange bias in a mixed oxide system. Typically, solutions of metal ion (Co(II)/Fe(II)) and oxidant (H_2O_2) were added via syringe pump to the apoferritin cages under an atmosphere of N_2 at pH 8.5 and elevated temperature (65 °C) over a defined time period (5 or 30 min). In the presence of apoferritin the reaction proceeded

(28) Mann, S.; Ozin, G. A. *Nature* **1996**, *382*, 313.
(29) Meldrum, F. C.; Heywood, B. R.; Mann, S. *Science* **1992**, *257*, 522.
(30) (a) Douglas, T.; Young, M. *Science* **2006**, *312*, 873. (b) Shenton, W.; Douglas, T.; Young, M.; Stubbs, G.; Mann, S. *Adv. Mater.* **1999**, *11*, 253.
(31) Allen, M.; Willits, D.; Mosolf, J.; Young, M.; Douglas, T. *Adv. Mater.* **2002**, *14*, 1562.
(32) McMillan, R. A.; Paavola, C. D.; Howard, J.; Chan, S. L.; Zaluzec, N. J.; Trent, J. D. *Nat. Mater.* **2002**, *1*, 247.
(33) Bulte, J. W. M.; Douglas, T.; Mann, S.; Frankel, R. B.; Moskowitz, B. M.; Brooks, R. A.; Baumgarner, C. D.; Vymazal, J.; Frank, J. A. *Invest. Radiol.* **1994**, *29*, S214.
(34) Bulte, J. W. M.; Douglas, T.; Mann, S.; Frankel, R. B.; Moskowitz, B. M.; Brooks, R. A.; Baumgarner, C. D.; Vymazal, J.; Strub, M. P.; Frank, J. A. *J. Magn. Reson. Imaging* **1994**, *4*, 497.
(35) Gider, S.; Awschalom, D. D.; Douglas, T.; Mann, S.; Chaparala, M. *Science* **1995**, *268*, 77.
(36) Gider, S.; Awschalom, D. D.; Douglas, T.; Wong, K.; Mann, S.; Cain, G. *J. Appl. Phys.* **1996**, *79*, 5324.
(37) Pankhurst, Q. A.; Betteridge, S.; Dickson, D. P. E.; Douglas, T.; Mann, S.; Frankel, R. B. *Hyperfine Interact.* **1994**, *91*, 847.
(38) Wong, K. K. W.; Douglas, T.; Gider, S.; Awschalom, D. D.; Mann, S. *Chem. Mater.* **1998**, *10*, 279.
(39) Resnick, D. A.; Gilmore, K.; Idzerda, Y. U.; Klem, M. T.; Allen, M.; Douglas, T.; Young, M.; Arenholz, E. *J. Appl. Phys.* **2006**, *99*, 08Q501.
(40) Mackle, P.; Charnock, J. M.; Garner, C. D.; Meldrum, F. C.; Mann, S. *J. Am. Chem. Soc.* **1993**, *115*, 8471.
(41) Mann, S. *Nature* **1991**, *349*, 285.
(42) Meldrum, F. C.; Douglas, T.; Levi, S.; Arosio, P.; Mann, S. *J. Inorg. Biochem.* **1995**, *58*, 59.
(43) Warne, B.; Kasyutich, O. I.; Mayes, E. L.; Wiggins, J. A. L.; Wong, K. K. W. *IEEE Trans. Magn.* **2000**, *36*, 3009.
(44) Ueno, T.; Suzuki, M.; Goto, T.; Matsumoto, T.; Nagayama, K.; Watanabe, Y. *Angew. Chem., Int. Ed.* **2004**, *43*, 2527.
(45) Kramer, R. M.; Li, C.; Carter, D. C.; Stone, M. O.; Naik, R. R. *J. Am. Chem. Soc.* **2004**, *126*, 13282.
(46) Wong, K. K. W.; Mann, S. *Adv. Mater.* **1996**, *8*, 928.
(47) Yamashita, I.; Hayashi, J.; Hara, M. *Chem. Lett.* **2004**, *33*, 1158.
(48) Iwahori, K.; Yoshizawa, K.; Muraoka, M.; Yamashita, I. *Inorg. Chem.* **2005**, *44*, 6393.
(49) Nedoloujko, A.; Kiwi, J. *J. Photochem. Photobiol., A* **1997**, *110*, 149.
(50) Finsy, R. *Adv. Colloid Interface Sci.* **1994**, *52*, 79.

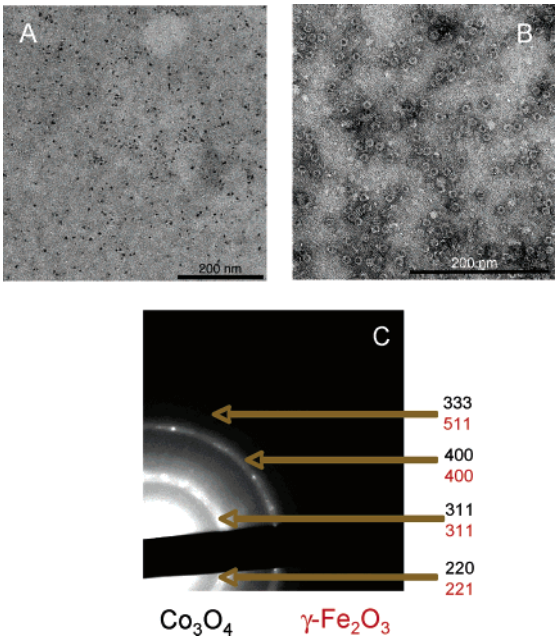

Figure 1. (A) Transmission electron micrograph of a mixed Fe/Co oxide mineralized inside the protein cage ferritin. (B) Transmission electron micrograph of a mixed Fe/Co oxide mineralized ferritin stained with 2% uranyl acetate. (C) Electron diffraction pattern of the mixed Fe/Co oxide mineralized inside the protein cage ferritin. The lattice indices in red correspond to Fe_3O_4, and black indices correspond to Co_3O_4.

to form a homogeneous dark brown solution, while control reactions performed in the absence of ferritin resulted in bulk precipitation of a dark brown solid. Dynamic light scattering of the ferritin reaction showed no apparent change in particle diameter suggesting that the oxides were encapsulated within the protein cage ferritin. The lack of precipitation and the absence of any change in the exterior diameter of the protein cage suggest that the reaction has occurred in a spatially selective manner within the ferritin cage.

Ferritin has previously been shown to be an excellent reaction vessel for controlled deposition inorganic nanoparticles of both iron[29,33−38] and cobalt oxides.[24,39] Here we have demonstrated that using ferritin under mild biomimetic reaction conditions, we can control mixed mineralization reactions of cobalt and iron oxides that lead to composite materials with unique and enhanced magnetic properties. This level of control can be achieved by the inherent stability of the cagelike architecture of ferritin under the reaction conditions and the ability to synthetically manipulate particle synthesis.

The products of the mineralization reactions were characterized by TEM and showed clear electron dense cores of a size consistent with the interior diameter of the protein cage (Figure 1a). The particle sizes were measured and found to be fairly monodispersed with an average diameter of 6.8−7.4 nm for the sample set (Table 1). When negatively stained with uranyl acetate, the intact protein cage was clearly visible as a white "halo" surrounding the metal oxide cores on the interior surface (Figure 1b). Selected area electron diffraction experiments on all samples that were doped with Co indicated that the materials were crystalline (Figure 1c displays the 33% Co doping) and revealed *d*-spacings that were consistent with both the spinel phase of cobalt oxide (Co_3O_4) and the inverse spinel magnetite (Fe_3O_4) but excluded cobalt monoxide (CoO) as a major

Table 1. Nanoparticle Diameter, As Determined by Transmission Electron Microscopy of Mixed Fe/Co Oxides Inside the Protein Cage Ferritin[a]

Co doping ratio in Fe_3O_4	diameter (nm)
0% Co (15 min)	7.0 ± 0.5
5% Co (15 min)	7.2 ± 0.5
10% Co (15 min)	7.4 ± 0.7
33% Co (5 min)	7.2 ± 0.8
33% Co (30 min)	6.9 ± 0.9
100% Co (15 min)	6.8 ± 0.6

[a] Synthesis time is denoted in parentheses.

contributor. On the basis of these data alone an unambiguous phase assignment could not be made.

To verify the cobalt oxide and iron oxide components of the electron diffraction, X-ray absorption spectroscopy (XAS) was performed to look at each component of the oxide in an element specific manner for comparison with reference XAS spectra. Examination of samples where the Co/Fe ratio had been varied from 0.05 to 0.33 in the synthesis yielded Fe L_3 and L_2 edge spectra (700−730 eV) that were all identical. Similarly, mineralized ferritin samples with Co/Fe ratios of 0.33 but synthesized under fast (5 min) and slow (30 min) synthesis conditions displayed the same Fe L_3 and L_2 edge spectra (shown in Figure 2A) as pure Fe_3O_4 mineralized in ferritin or with a $CoFe_2O_4$ standard for the Fe (there is no clear spectral difference for Fe in these two structures). In each case, the collected spectra were consistent with Fe in a local environment of $Co_xFe_{3-x}O_4$ ($x = 0-0.33$) across all dopant levels.

The Co L_3 and L_2 edges (775−802 eV) for a Co/Fe ratio of 0.33 yielded spectra whose shapes were dependent on the synthesis time. Co was incorporated into each nanoparticle in two competing phases, Co_3O_4 or $CoFe_2O_4$ (where there is a clear spectral difference for Co in these two structures as demonstrated in the bottom spectra of Figure 2B). When the synthesis time was fast (5 min), the spectra exhibited line shapes consistent with nanoparticles with Co in two distinct phases, Co_3O_4 and $CoFe_2O_4$. A comparison of the measured spectra with a normalized sum of the two reference spectra was consistent with a nanoparticle composed of 85% $CoFe_2O_4$ and 15% of Co_3O_4 (top spectra of Figure 2B). When the synthesis time was extended to 30 min (slow), the observed spectra had undergone a dramatic change. This spectrum could be accounted for by summing standard spectra of $CoFe_2O_4$ and Co_3O_4 with a weighting of 25% and 85%, respectively (middle spectra of Figure 2B).

The Fe spectra are clear indicators that the Fe remains in the inverse spinel structure type of Fe_3O_4, whereas, with increasing Co concentration, the Co XAS spectra indicate that the Co either occupies Fe^{2+} site to give a material whose composition is $Co_xFe_{3-x}O_4$ ($x = 0-0.33$) or shifts toward Co(III) through the formation of Co_3O_4 depending on synthesis time. This valance variation clearly indicates that the Co is not fully incorporated into the iron oxide host but rather is formed as a second antiferromagnetic phase, which can lead to a substantial magnetic exchange bias of the ferrimagnetic $Co_xFe_{3-x}O_4$ oxide by the antiferromagnetic Co_3O_4 in the case of a slow synthesis.

To study the interaction between these two magnetic phases, the magnetic blocking temperatures of the nanoparticles (summarized in Table 2) were determined for the series of particles of various composition by determining the maxima in the

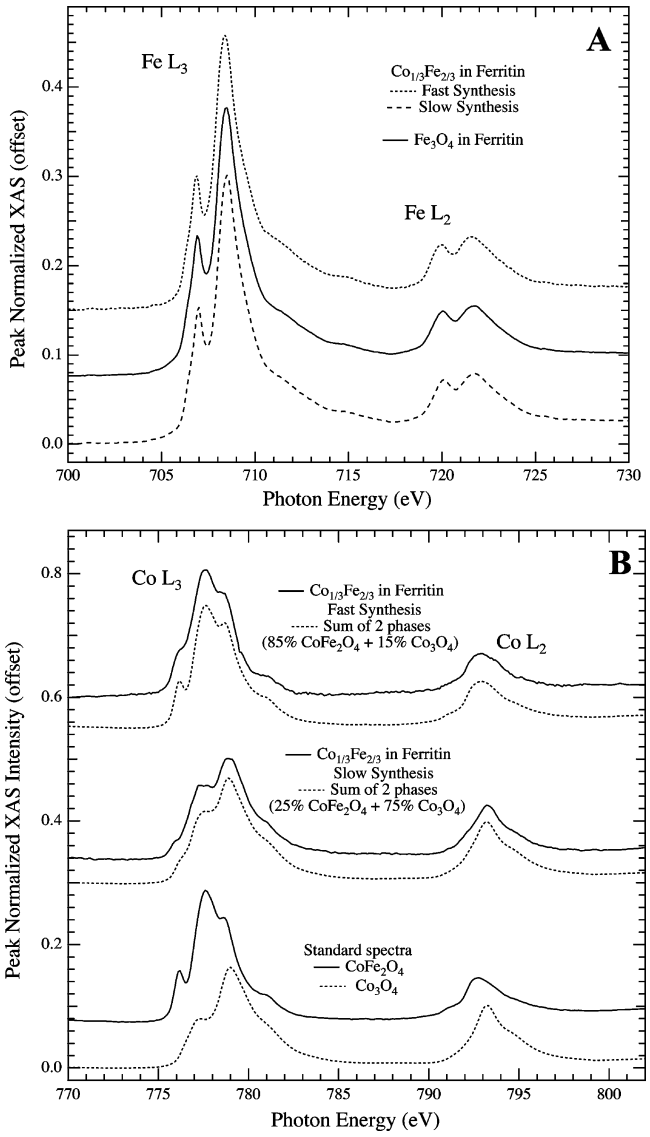

Figure 2. X-ray absorption spectra of both the (A) Fe and (B) Co $L_{2,3}$-edges for the mixed $Co_{1/3}Fe_{2/3}$ oxide mineralized ferritin. Panel A displays the Fe XAS spectra for the slow and fast synthesis (dashed lines) as well as the Fe spectra for pure Fe_3O_4 mineralized in ferritin (solid line). The spectra are identical. Panel B displays the Co XAS spectra (offset for clarity) for the fast (top solid line) and slow synthesis (middle solid line) as well as the Co spectra for pure $CoFe_2O_4$ (bottom solid line) and Co_3O_4 (bottom dashed line). Immediately under the experimental spectra are weighted summed spectra (dashed lines) of the two standard materials which best reproduce the data.

Table 2. Coercive Fields and Ferromagnetic Blocking Temperatures for a Series of Fe and Co Materials[a]

mineral in ferritin	H_c at 5 K (kG)	T_B (K)
Co_3O_4	0.140	4.2
Fe_3O_4	1.2	30
5% Co in Fe_3O_4	8.2	76
10% Co in Fe_3O_4	7.2	126
33% Co in Fe_3O_4 fast synthesis	8.3	50
33% Co in Fe_3O_4 slow synthesis	7.8	60

[a] The blocking temperature was determined by ACMS with a measurement frequency of 1 kHz.

imaginary component of the ac susceptibility. The blocking temperatures showed a dramatic variation as the Co/Fe ratio was increased, as compared to either pure Fe_3O_4 ($T_b = 30$ K) or Co_3O_4 ($T_b = 4.2$ K) particles synthesized in the same manner

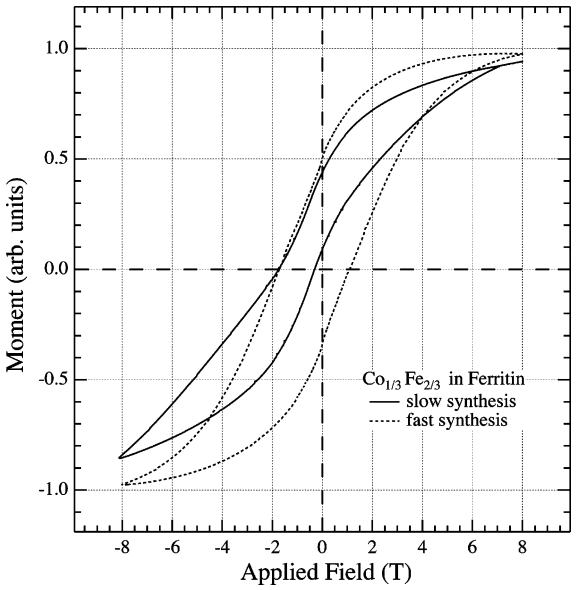

Figure 3. Hysteresis loops measured at 2 K for field-cooled (−8 T) mixed oxide material with nominal composition 66% Fe_3O_4 and 33% Co_3O_4 for slow (solid) and fast (dashed) synthesis. The offset between the two hysteresis loops is the exchange bias.

within the ferritin cage. The blocking temperature more than doubled at 5% Co/Fe ($T_b = 76$ K) and quadrupled at 10% Co/Fe ($T_b = 126$ K). At a Co/Fe ratio of 33% the composite material exhibited a reduced blocking temperature ($T_b = 60$ K) that was still double that of Fe_3O_4 synthesized previously in ferritin.[51]

Clearly, the enhancement in the magnetic anisotropy and corresponding increase in blocking temperature were due to the introduction of Co into the synthetic reaction, and it was hypothesized that this phenomenon was a consequence of Co being incorporated into the Fe_3O_4 lattice. The decreasing trend in T_B observed after 10% Co/Fe results from the formation of phase-segregated oxides (Fe and Co) supported by the dramatic increase in exchange bias at 33% Co/Fe which resulted from the interaction between the ferrimagnetic (Fe_3O_4) and antiferromagnetic (Co_3O_4) particles within the protein cage. When the synthesis time was varied from 5 to 30 min, the blocking temperature showed only minor changes (50 K at 5 min synthesis and 60 K for 30 min synthesis) and only a small change in the coercive field at 5 K (8.3 vs 7.8 kG).

The magnetic properties of the nanoparticles were studied by measuring the magnetization as a function of field at various temperatures from 4 to 300 K. When the samples were cooled, in the presence of an 8 T applied field, across the Néel temperature (T_N) of Co_3O_4, the exchange bias was clearly revealed (shown in Figure 3). This is strong evidence that the particles are composed of two intimately connected materials, a ferrimagnetic core in direct contact with an antiferromagnetic component which serves as an exchange bias layer. At low temperatures ($T < 30$ K) all samples displayed an exchange bias in the hysteresis loop and an increase in the coercive fields (H_c, Table 2). The hysteresis loops for 33% Co/Fe cooled in a positive and negative applied field are shown in Figure 3. At 5 K the exchange bias effect is clearly evident by the large offset in the hysteresis loops representing an exchange field up to 10.8 kG for the slow synthesis. For the slowly synthesized particles

(51) Resnick, D.; Gilmore, K.; Idzerda, Y. U.; Klem, M.; Smith, E.; Douglas, T. *J. Appl. Phys.* **2004**, *95*, 7127.

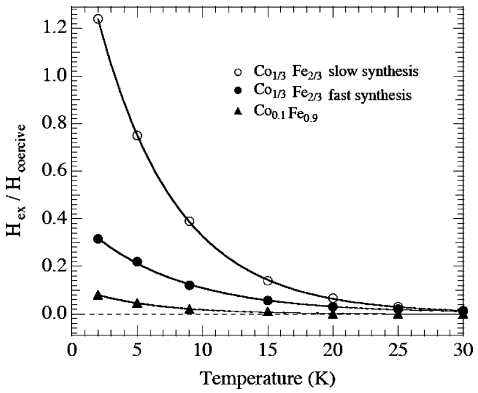

Figure 4. Temperature dependence of the exchange bias for a slow synthesized 33% Co (open circle), fast synthesized 33% Co (filled circle), and 10% Co (filled triangle) in Fe_3O_4. In all cases the exchange bias vanishes at 30 K.

(30 min), the measured H_{ex}/H_c ratio of 1.3 at 2 K is one of the largest reported for nanoparticles (see Figure 4).[52−54] When the reaction time was shortened to 5 min, the measured H_{ex}/H_c ratio was reduced to only 0.3. This drop in exchange bias is due to Co being incorporated into the rapidly forming Fe_3O_4 lattice reducing the amount of antiferromagnetic Co_3O_4 available to bias the Fe_3O_4 core.

The temperature dependence of the exchange bias of 10% and 33% Co/Fe, shown in Figure 4 is consistent with the view that the particles are phase separated between a ferrimagnetic iron oxide particle in direct contact with an antiferromagnetic cobalt oxide which is the source of the exchange bias. In each case there is a rapid decrease in the H_{ex}/H_c ratio as the temperature is increased, and the exchange bias disappeared at 30 K, near the Néel temperature of Co_3O_4. The exchange bias was highest in the particles with a 33% Co/Fe loading ratio and synthesized slowly over a 30 min period, as expected, since there is more antiferromagnetic Co_3O_4 present to bias the ferrimagnetic Fe_3O_4 core.

The observed decrease in exchange bias with decreasing synthesis time is likely due to a number of factors that include kinetic and thermodynamic considerations. Under the fast synthetic conditions Co is most likely incorporated into the rapidly forming Fe_3O_4 lattice leading to an enhanced blocking temperature but with a loss of exchange bias properties. Under synthesis conditions where the reaction proceeds slowly, it is expected that Fe_3O_4 formation would precede the nucleation and growth of Co_3O_4 on the basis of standard reduction potentials of Fe^{3+} and Co^{3+} (0.771 and 1.808, respectively) resulting in a composite material that is mixed phase leading to an increase in the exchange bias behavior. Regardless, the experimental evidence indicates fast synthesis leads to Co incorporation as a $Co_xFe_{3-x}O_4$ oxide whereas slow synthesis results in a larger fraction of Co in the Co_3O_4 phase in the composite nanoparticle.

Conclusions

Ferritin had previously been shown to be an excellent reaction vessel for controlled deposition of inorganic nanoparticles of both iron and cobalt oxides. Here we demonstrate that using ferritin under mild biomimetic reaction conditions we can control mixed mineralization reactions of cobalt and iron oxides that lead to composite materials with tailored magnetic properties.

The ability to control the resulting magnetic behavior of synthesized nanoparticles is important in magnetic device applications. This work illustrates the use of a biomimetic synthesis route in the formation of magnetic nanoparticles with controlled composite ferri- and antiferromagnetic properties. We have demonstrated exchange bias as a mechanism for enhancing the magnetic response as a function of temperature in a composite nanoparticle. The properties of a $Co_3O_4/Co_xFe_{3-x}O_4$ nanoparticle assembly was studied as a function of Co/Fe loading, and the ability to tune the magnetic properties, particularly the exchange bias, as a function of Co loading was also demonstrated.

This work also highlights the usefulness of empty protein cages as constrained reaction vessels for the synthesis of nanomaterials using nonnative precursors, under mild synthetic conditions. The synthesized materials are both size and shape constrained by the interior volume of the protein cage. Previous work has suggested that the use of protein cages in the synthesis of magnetic nanoparticles yields an ensemble of noninteracting magnetic nanoparticles.[39,51,55] This biomimetic approach allows for a controlled study of the physical properties of these protein−nanomaterial composites. Our results also suggest the potential for nanomaterial synthesis using an increasingly diverse library of protein cages as size-constrained templates.[56]

Acknowledgment. This research was supported in part by grants from the National Science Foundation (0103509 and NIRT-DMR0210915), Office of Naval Research (19-00-R006 and N00014-03-1-0692), and National Institutes of Health (1R21EB005364-01). The ALS and NSLS are supported by the Department of Energy.

JA0667561

(52) Riveiro, J. M.; De-Toro, J. A.; Andres, J. P.; Gonzalez, J. A.; Munoz, T.; Goff, J. P. *Appl. Phys. Lett.* **2005**, *86*, 172503
(53) Vazquez, M.; Luna, C.; Morales, M. P.; Sanz, R.; Serna, C. J.; Mijangos, C. *Physica B* **2004**, *354*, 71.
(54) Skumryev, V.; Stoyanov, S.; Yong, Z.; Hadjipanayis, G.; Givord, D.; Nogues, J. *Nature* **2003**, *423*, 850.
(55) Gilmore, K.; Idzerda, Y. U. K., M. T.; Allen, M.; Douglas, T. Y. M. *J. Appl. Phys.* **2005**, 97, 10B301.
(56) Klem, M. T.; Young, M.; Douglas, T. *Mater. Today* **2005**, *8*, 28.